

General relativistic numerical simulation of sub-Keplerian transonic accretion flows on to rotating black holes: Kerr space–time

Jinho Kim,^{1,2} Sudip K. Garain,^{2*} Sandip K. Chakrabarti^{3,4} and Dinshaw S. Balsara²

¹*Korea Astronomy & Space Science Institute, 776 Daedeokdae-ro, Yuseong-gu, Daejeon 34055, Korea*

²*Department of Physics, University of Notre Dame, Notre Dame, IN 46556, USA*

³*S. N. Bose National Center for Basic Sciences, Block JD, Sector III, Salt Lake, Kolkata 700098, India*

⁴*Indian Center for Space Physics, 43 Chalantika, Garia St. Rd., Kolkata 700084, India*

Accepted 2018 October 26. Received 2018 October 19; in original form 2018 June 24

ABSTRACT

We study time evolution of sub-Keplerian transonic accretion flows on to black holes using a general relativistic numerical simulation code. We perform simulations around the black holes having non-zero rotation. We first compare one-dimensional simulation results with theoretical results and validate the performance of our code. Next, we present results of axisymmetric, two-dimensional simulation of advective flows. In the literature, there is no solution which describes steady shock solutions in two dimensions. However, our simulations produce these centrifugal force supported steady shock waves even in presence of strong dragging of inertial frames. Since the post-shock region could be hot and upscatter photons through Comptonization, these shock would put imprints on the spectra. Thus, our solutions, which represent truly new results, could be useful to measure spins through radiation spectrum of accreting Kerr black holes.

Key words: accretion, accretion discs – black hole physics – hydrodynamics – shock waves – methods: numerical.

1 INTRODUCTION

Matter from a companion star in a binary system spirals towards the primary through a process known as accretion. In the case of high viscosity, matter injected at the outer boundary would form a Keplerian disc before entering into the black hole (Chakrabarti 1996b). In this paper, we study what happens when an inviscid flow of low-angular momentum matter spirals into a rotating black hole, space–time geometry around which is the well-known Kerr geometry. A low-angular momentum matter would feel the centrifugal barrier ($\sim l^2/r^3$, l and r being the specific angular momentum and the radial distance, respectively) and would slow down, and pile up eventually making a possible density jump, before entering the black hole. This is a possibility for inviscid flow, though in presence of viscosity the result depends on the exact magnitude of viscosity. These shock waves, just outside the horizon provides an opportunity to study the emission of radiation in a strong gravity limit and would therefore be of great interest, especially to pinpoint the mass and the spin of the central object.

In the two-component advective flow (TCAF) scenario (Chakrabarti & Titarchuk 1995, and references therein), the soft photons from the Keplerian disc are intercepted by the post-shock

region and leave the system as hard radiation. The oscillations of the post-shock region will leave its signature in the outgoing hard photons. It has been shown using numerical simulations and theoretical work (Molteni, Sponholz & Chakrabarti 1996; Chakrabarti, Acharyya & Molteni 2004; Garain, Ghosh & Chakrabarti 2014; Chakrabarti, Mondal & Debnath 2015) that when there is a resonance between the infall time-scale (compressional heating) and the cooling time-scale, the shock surface oscillates at a particular frequency which is approximately inverse to the infall (or, cooling) time-scale. It was further shown in Garain et al. (2014) that the resulting light curves exhibit quasi-periodic oscillations (QPOs) and the frequency of the QPOs are consistent with the infall time-scales (see also Chakrabarti et al. 2015). Since the infall time-scale is proportional to the (radius)^{3/2} of the shock, larger shock radius produces lower QPO frequency. In fact, TCAF model has been added as a local additive table model into HEASARC’s spectral analysis software package XSPEC. Consequently, for outbursting sources where QPO frequency starts from mHz and continue to increase to a few tens of Hz, it has been found that the shock forms far away from the black hole initially and then propagates towards to black hole during the rising phase (Debnath, Chakrabarti & Mondal 2014; Chatterjee et al. 2016; Bhattacharjee et al. 2017; Debnath et al. 2017). In the declining phase, the opposite phenomena occurs, namely, the shock recedes and the QPO frequency steadily goes down. Several physical parameters associated with the accretion discs such as accretion

* E-mail: sgarain@nd.edu

rates, mass of the black holes, shock locations, and the strength of the shock are found by analysing the data for various sources (see above references).

Global solutions of weakly viscous transonic flows in Kerr geometry have been found in great detail by Chakrabarti (1996a,c). Complete theoretical studies for accretion and winds are obtained assuming the flow to be in vertical equilibrium (VE) or in the form of conical wedge (CF). It was found that for a large region of the parameter space in each model, a shock wave will form as a distance depending on the conserved energy, angular momentum, and spin parameters. These solutions give the closest possible description to an actual flow dynamics, since a low-angular momentum flow is likely to be geometrically thick and quasi-spherical far away from the black hole. However, theoretical works cannot be done in such cases.

In this paper, we concentrate on the numerical simulations of these flow in a complete Kerr geometry. Our goal is first to see if the theoretical results mentioned above are instead stable. This is because of the fact that a flow actually slows down to a large extent in the post-shock region, just outside the horizon, itself is very exciting and it would be important to throw light on their stability properties. Second, we would also like to prove the effects of the dragging of inertial frames and eventually, whether such effects cause precession of outflows and jets. So the code must be tested against known theoretical solutions. We will test the code for a conical flow for simplicity. Since the relevant equations are given in Chakrabarti (1996a,c), we do not repeat them here. Instead we only mention the key points.

In this paper, we choose $R_g = GM_{\text{BH}}/c^2$ as the unit of length, R_g/c as unit of angular momentum, and R_g/c as unit of time. In addition, we choose the geometric units $G = M_{\text{BH}} = c = 1$ (G is gravitational constant, M_{BH} is the mass of the central black hole, and c is the unit of light). Thus $R_g = 1$, and angular momentum and time are measured in dimensionless units.

2 ANALYTICAL SOLUTION

We assume a thin conical wedge shaped adiabatic flow symmetrically placed on both sides of the equatorial plane, $\theta = \pi/2$, entering into a Kerr black hole. For analytical studies, we assume the Kerr metric transformed to the cylindrical coordinate which is written as follows (Novikov & Thorne 1973):

$$ds^2 = g_{\mu\nu} dx^\mu dx^\nu = -\frac{r^2 \Delta}{A} dt^2 + \frac{A}{r^2} (d\phi - \omega dt)^2 + \frac{r^2}{\Delta} dr^2 + dz^2. \quad (1)$$

Here,

$$A = r^4 + r^2 a^2 + 2ra^2, \quad \Delta = r^2 - 2r + a^2, \quad \omega = 2ar/A,$$

a being the spin parameter of the black hole and ω represents the frame dragging due to the rotation of the central black hole.

In absence of viscosity and any heating or cooling, one can find the conserved specific energy as (Chakrabarti 1996c)

$$\epsilon = hu_t = \frac{1}{1 - na_s^2} u_t, \quad (2)$$

where, $n = 1/(\Gamma - 1)$ is the polytropic index, Γ being the adiabatic index, and $h = 1/(1 - na_s^2)$ is the enthalpy, a_s being the sound speed. Also,

$$u_t = \left[\frac{\Delta}{(1 - V^2)(1 - \Omega l)(g_{\phi\phi} + l g_{t\phi})} \right]^{1/2}. \quad (3)$$

Here,

$$\Omega = \frac{u^\phi}{u^t} = -\frac{g_{t\phi} + l g_{tt}}{g_{\phi\phi} + l g_{t\phi}}, \quad (4)$$

and $l = -u_\phi/u_t$ is the specific angular momentum. Also,

$$V = \frac{\mathcal{V}}{(1 - \Omega l)^{1/2}}, \quad (5)$$

where

$$\mathcal{V} = \left(-\frac{u_r u^r}{u_t u^t} \right)^{1/2}. \quad (6)$$

We rewrite equation (2) as

$$\epsilon = \frac{1}{1 - na_s^2} \frac{1}{(1 - V^2)^{1/2}} F(r), \quad (7)$$

where,

$$F(r) = \left[\frac{\Delta}{(1 - \Omega l)(g_{\phi\phi} + l g_{t\phi})} \right]^{1/2}.$$

The entropy accretion rate (Chakrabarti 1989, 1996c) can be obtained as

$$\dot{m} = \left(\frac{a_s^2}{1 - na_s^2} \right)^n \frac{V}{(1 - V^2)^{1/2}} G(r), \quad (8)$$

where, $G(r) = r\Delta^{1/2}$.

We follow the standard solution procedures (Chakrabarti 1996a,c) to calculate $V(r)$ and radial dependence of other required quantities. By differentiating equations (7) and (8) with respect to r and eliminating terms involving da_s/dr , we find following expression as the gradient of $V(r)$:

$$\frac{dV}{dr} = \frac{V(1 - V^2)[a_s^2 R_1 - R_2]}{(V^2 - a_s^2)}, \quad (9)$$

where, $R_1 = \frac{1}{G(r)} \frac{dG(r)}{dr}$ and $R_2 = \frac{1}{F(r)} \frac{dF(r)}{dr}$.

At the sonic point, both numerator and the denominator vanish and one obtains the so-called sonic point condition as

$$V_c = a_{s,c}; \quad a_{s,c}^2 = \frac{R_2}{R_1} \Big|_c. \quad (10)$$

Here, subscript c refers to the quantities evaluated at the sonic point $r = r_c$.

To find a complete solution from the horizon to infinity for a given black hole spin parameter a , one needs to supply the specific energy ϵ and the specific angular momentum l . For Kerr black holes, a few examples of classification of parameter space spanned by these two parameters, namely ϵ and l , has been provided in Chakrabarti (1996a,c). The accretion or wind solutions may pass through one or multiple sonic points. Moreover, a solution having more than one sonic points may form a standing shock. The location of the shock may be found by solving continuity of energy equation, mass flux equation, and relativistic momentum balance condition simultaneously. These are collectively called the ‘shock conditions’. For more discussions on these solutions, readers are referred to the aforementioned references. In this paper, we obtain shock locations in some flow parameters and compare the results of numerical simulations to see if the shocks indeed form in a realistic flow.

3 NUMERICAL SIMULATION PROCEDURE

In this section, we describe how we can obtain the time dependent numerical solution using the boundary condition provided in Sec-

tion 2. Instead of the space–time metric provided in equation (1) we use the usual Boyer–Lindquist coordinates (t, r, θ, ϕ) for the Kerr metric for the numerical simulation (Boyer & Lindquist 1967). In the ADM 3 + 1 decomposition, the space–time is expressed in terms of the lapse (α) , shift (β^i) , and spatial metric (γ_{ij}) (Arnowitt, Deser & Misner 2008). The line element around Kerr black hole can be expressed as follows:

$$\begin{aligned} ds^2 &= -\alpha^2 dt^2 + \gamma_{ij} (dx^i + \beta^i dt) (dx^j + \beta^j dt) \\ &= -\left(1 - \frac{2r}{\rho^2}\right) dt^2 - \frac{4ar \sin^2 \theta}{\rho^2} dt d\phi \\ &\quad + \frac{\rho^2}{\Delta} dr^2 + \rho^2 d\theta^2 + \frac{\Sigma}{\rho^2} \sin^2 \theta d\phi^2, \end{aligned} \quad (11)$$

where

$$\begin{aligned} \rho^2 &= r^2 + a^2 \cos^2 \theta, \\ \Delta &= r^2 - 2r + a^2, \\ \Sigma &= (r^2 + a^2)^2 - a^2 \Delta \sin^2 \theta. \end{aligned}$$

Then, the lapse, α , and shift, β^i , in equation (11) are

$$\begin{aligned} \alpha &= \sqrt{\frac{\rho^2 \Delta}{\Sigma}}, \\ \beta^r &= \beta^\theta = 0, \quad \beta^\phi = -\frac{2ar}{\Sigma}. \end{aligned} \quad (12)$$

In this paper, we do not consider the evolution of the space–time metric by the influence of the accreting matter. In other words, we assume that the accretion mass is too light to affect the space–time metric of the central black hole. For typical accretion disc around a central black hole of Mass $10 M_\odot$, the mass accretion rate (\dot{M}) of one Eddington rate, when expressed in the unit of M_\odot , comes out to be $\sim 10^{-15} M_\odot \text{ s}^{-1}$. Such a small accretion rate cannot increase the mass or change the angular momentum of the central black hole within our simulation time (\sim a few 10 ms). Therefore, we can rightly neglect the self-gravity of the disc.

For the evolution of the accreting matter (hydrodynamic simulation), we adopt the Valencia formulation which is written as a flux conservative form in the 3 + 1 decomposition of space–time (Banyuls et al. 1997). In our coordinate system, the conservative (q) and primitive (w) variables are,

$$q = \begin{pmatrix} D \\ S_r \\ S_\theta \\ S_\phi \\ \tau \end{pmatrix} = \begin{pmatrix} \rho_0 W \\ \rho_0 h W^2 v_r \\ \rho_0 h W^2 v_\theta \\ \rho_0 h W^2 v_\phi \\ \rho_0 h W^2 - P - D \end{pmatrix}, \quad w = \begin{pmatrix} \rho_0 \\ v^r \\ v^\theta \\ v^\phi \\ P \end{pmatrix}. \quad (13)$$

Here, ρ_0 is the fluid rest mass density, P is the pressure, and h is the specific enthalpy. They are measured in the co-moving frame of the fluid. v^i is the fluid velocity measured by Eulerian reference frame i.e., $v^i = \frac{u^i}{\alpha u^t} + \frac{\beta^i}{\alpha}$. W is the Lorentz factor and defined as $W = \alpha u^t = 1/\sqrt{1 - \gamma_{ij} v^i v^j}$. Here, γ_{ij} are the spatial part of the metric components $g_{\mu\nu}$. The radial and angular velocity in the Eulerian frame can be expressed in terms of \mathcal{V} in equation (6) and Ω in equation (4),

$$\begin{aligned} v^r &= \sqrt{-\frac{g_{tt} + g_{t\phi}\Omega}{g_{rr}\alpha^2}} \mathcal{V}, \\ v^\phi &= \frac{1}{\alpha} (\Omega - \beta^\phi). \end{aligned} \quad (14)$$

Assuming axisymmetry ($\frac{\partial}{\partial \phi} = 0$), the hydrodynamic equations in the curved space–time that are described in equation (11) can be

written as follows:

$$\frac{\partial (\sqrt{\gamma} q)}{\partial t} + \frac{\partial (\sqrt{-g} f^r)}{\partial r} + \frac{\partial (\sqrt{-g} f^\theta)}{\partial \theta} = \sqrt{-g} S, \quad (15)$$

where

$$\begin{aligned} f^r &= \begin{bmatrix} D v^r \\ S_r v^r + P \\ S_\theta v^r \\ S_\phi v^r \\ \tau v^r + P v^r \end{bmatrix}, \\ f^\theta &= \begin{bmatrix} D v^\theta \\ S_r v^\theta \\ S_\theta v^\theta + P \\ S_\phi v^\theta \\ \tau v^\theta + P v^\theta \end{bmatrix}, \\ S &= \begin{bmatrix} 0 \\ \frac{1}{2} T^{\mu\nu} \partial_r g_{\mu\nu} \\ \frac{1}{2} T^{\mu\nu} \partial_\theta g_{\mu\nu} \\ 0 \\ \alpha (T^{\mu t} \partial_\mu (\ln \alpha) - T^{\mu\nu} \Gamma_{\mu\nu}^t) \end{bmatrix}. \end{aligned} \quad (16)$$

Here $T^{\mu\nu}$ is the stress energy tensor of the perfect fluid which is defined as $T^{\mu\nu} = \rho_0 h u^\mu u^\nu + P g^{\mu\nu}$. $\sqrt{\gamma}$ and $\sqrt{-g}$ are the determinants of spatial and space–time metric, respectively. From the Kerr metric shown in equation (11), we have

$$\sqrt{\gamma} = \sqrt{\frac{\rho^2 \Sigma}{\Delta}} \sin \theta, \quad \sqrt{-g} = \alpha \sqrt{\gamma} = \rho^2 \sin \theta. \quad (17)$$

As we see in equation (16), this formulation is not strictly a flux conservative form due to the non-zero source terms in S . The source terms, however, contain spatial derivatives of the metric components only (they come from the Christoffel symbols) and they do not have any derivatives of the hydrodynamic variables. Note that even for the general time dependent metric, the time derivative of metric components can be substituted by their spatial derivatives from the Einstein equation. Therefore, the source term does not have time derivatives.

We use the ideal gas equation of state which can be written in the following form:

$$P = (\Gamma - 1) \rho_0 e, \quad (18)$$

where e is the specific internal energy. The above equation of state provides the expression of specific enthalpy,

$$h = 1 + \frac{\Gamma}{\Gamma - 1} \frac{P}{\rho_0}. \quad (19)$$

In this paper, we solve the hydrodynamic equations in (15) and (16) using a numerical code developed by Kim et al. (2012). The details of the code can be found in Kim et al. (2012). The most useful property of this code is that it can be applied to any space–time metric in any coordinate system. Although the original code by Kim et al. (2012) is written in the so-called ‘pseudo-Newtonian’ metric, we can easily apply the code to the Kerr geometry. This code uses finite volume method to enforce local conservation of the fluid in the computational grid. Therefore, the code can guarantee total mass and angular momentum conservations which appear in the first and fourth rows of equation (16). For the treatment of the discontinuous solution of the fluid such as shocks, rarefactions, or contact discontinuities, the High Resolution Shock Capturing (HRSC) techniques are applied in the code. We use the third order slope limiter proposed by Shibata (2003) which is based on the *minmod* function. For the flux approximation, we use the HLL method that takes care

of maximum and minimum wave speed (Harten, Lax & van Leer 1983). The HLL method has some dissipation but the results are very stable. For the time integration, we use the third order three stage Strong Stability-Preserving (SSP) Runge–Kutta method by using method of line. It is known as Shu–Osher method (Shu & Osher 1988).

4 RESULTS

4.1 One-dimensional conical accretion flow

First we test the code by reproducing theoretically obtained steady non-linear solutions using the code. We test for both the accretion and winds. In the first case, the accreting matter starts from a large distance and after passing through a sonic point, it passes through the standing shock where many of the flow variables jump abruptly. After that, it passes through another mandatory sonic point before disappearing behind the horizon supersonically. In the second case, the wind starts from an accretion flow and due to thermal pressure, it is pushed out to infinity after successively passing through the innermost sonic point, a shock, and the outer sonic point. The challenges faced by a code are to test if (i) the shocks are actually formed, and if yes, (ii) whether the jump in Mach number occurs in a very narrow region and exactly at the same place as predicted, since theoretically, the shocks in an inviscid flow are infinitesimally thin. Once the tests are successful, one could explore unknown territories, such as geometrically thick, fully two-dimensional flows.

In Fig. 1(a)–(c) we show the results of three numerical simulations for the prograde flows. There were 300 logarithmically spaced radial grids for all the one-dimensional simulations presented here. For accretion solutions, the outer and inner boundaries are located at $r_{\text{out}} = 200$ and $r_{\text{in}} = 1.2$, respectively. We use $a = 0.95$ for all three cases. In Fig. 1(a), we consider the flow parameter from the ‘No Shock in Accretion’ (NSA) region (fig. 2 of Chakrabarti 1996c). If a flow starts with parameters from this region, then the shock conditions are not satisfied and the flow passes through the outer sonic point and enters into the black hole smoothly. This particular case is with the parameter pair of $\varepsilon = 1.004$ and $l = 2.2$. The solid black curves give the theoretical distribution of the Mach number (V/a_s) as a function of the radial distance. The upper branch is complete in the sense that it connects the black hole horizon with a large distance, while the lower (subsonic) branch is an isolated solution which does not connect flows at a large distance. Red ‘+’ signs signify the results of numerical simulations. Matter is injected at $r_{\text{out}} = 200$ with the radial velocity and sound speed as in the theoretical solution. We find that the steady solution exactly matched with the theoretical solution branch.

In the next simulation (Fig. 1b), we choose the injected parameter from a region called ‘Shock in Accretion’ (SA) of Chakrabarti (1996c). We choose $\varepsilon = 1.004$ and $l = 2.25$ in this case. The analytical solution is exactly reproduced by the numerical simulation with the shock thickness about a grid size which is the smallest resolvable length scale. The shock is formed at $r = 4.05$. The reason why the flow chose to jump on the lower branch is that the entropy of the flow which passes through the inner sonic point is higher than that of the upper branch and flow chose that branch for stability. In Fig. 1(c), we carry out a simulation with flow parameters from the ‘Shock in Winds’ (SW) region. Here the parameters are $\varepsilon = 1.02$ and $l = 2.3$. The matter is injected from a radius $r_{\text{in}} = 1.5$ outwards on the equatorial plane assuming there is a matter source (such as a disc). It immediately passes through the sonic point, but reaches to a large distance only after passing through a shock wave.

When comparing with the theoretical solution, we note that there is a slight deviation at a large distance. On inspection, we find that this is due to finite resolution of the grid. A small error (which is equivalent to a large fractional error) in the location of shock wave (which is grid resolution limited) is propagated downstream and affect the numerical results. The error in thermodynamic quantities in the shock location does not propagate backward in the supersonic region, and thus does not affect the pre-shock branch at all. The shock is located at 2.77. Clearly the error would be reduced with the reduction of the grid size.

In Fig. 1(d), we present the results of our simulation for a retrograde accretion flow. We choose $\varepsilon = 1.004$, $l = 4.0$, and spin parameter $a = -0.95$ in this case. The outer and inner boundaries are located at $r_{\text{out}} = 200$ and $r_{\text{in}} = 1.6$, respectively. Analytical method predicts the shock to form at $r = 22.45$. As in the prograde flow, here also, we find the analytical solution is exactly reproduced by the numerical simulation with the shock thickness about a grid size.

4.2 Two-dimensional Bondi accretion flow

Having convinced ourselves that the numerical code has reproduced theoretical non-linear solution exactly, we turn our attention to solve the simplest possible two-dimensional problem which does not have any theoretical solution. For all the two-dimensional flows presented here, there were 300 logarithmically spaced radial grids and 90 equal spaced grids along the polar angle. We study the spherically symmetric flow (at a large distance) on a Kerr geometry which is a special case of Chakrabarti (1996c) solution for $l = 0$. Earlier Michel (1972) solved for Bondi flows on a Schwarzschild geometry which remained spherically symmetric even on the horizon. However, as we show below, due to the dragging of inertial frame the flow becomes necessarily axisymmetric rather than spherically symmetric close to the black hole. Our goal would be to see how the dragging of the inertial frame would modify the symmetry of the flow.

To show the effects of dragging of frames due to spin of the black hole, we run the same case twice: for the Kerr ($a = 0.95$) and the Schwarzschild ($a = 0$) geometries and then take the difference in density distribution in the two cases. We injected matter with radial velocity 0.02288 and sound speed 0.08053 at $r_{\text{out}} = 200$ (Kim et al. 2017). However, for Schwarzschild black hole case, the inner boundary is placed at $r_{\text{in}} = 2.1$ and for Kerr black hole, $r_{\text{in}} = 1.5$.

In Fig. 2(a), we plot colours of the density difference. We see that the difference is higher along the axis. This is expected since the effects of spin on space–time is the highest at the pole. In Fig. 2(b), we plot the ratio of the radial distance for a given density divided by that on the polar axis as a function of the polar angle. The contours of density 50, 100, 150, 200, and 250 are shown (from bottom to top). Clearly, higher the density, i.e., closer the flow to the horizon, the difference between the equatorial value and axial values are higher. Dragging of the inertial frame induces a little rotation ($\Omega \sim 2.375 \times 10^{-7}$) at the outer boundary of the grid on the equatorial plane where $r = 200$.

4.3 Two-dimensional accretion flow with non-zero angular momentum

We now apply the code to a more complex case where the accreting matter has some angular momentum. Such situations occur in wind-fed systems as in Cygnus X-1. In the context of pseudo-Newtonian

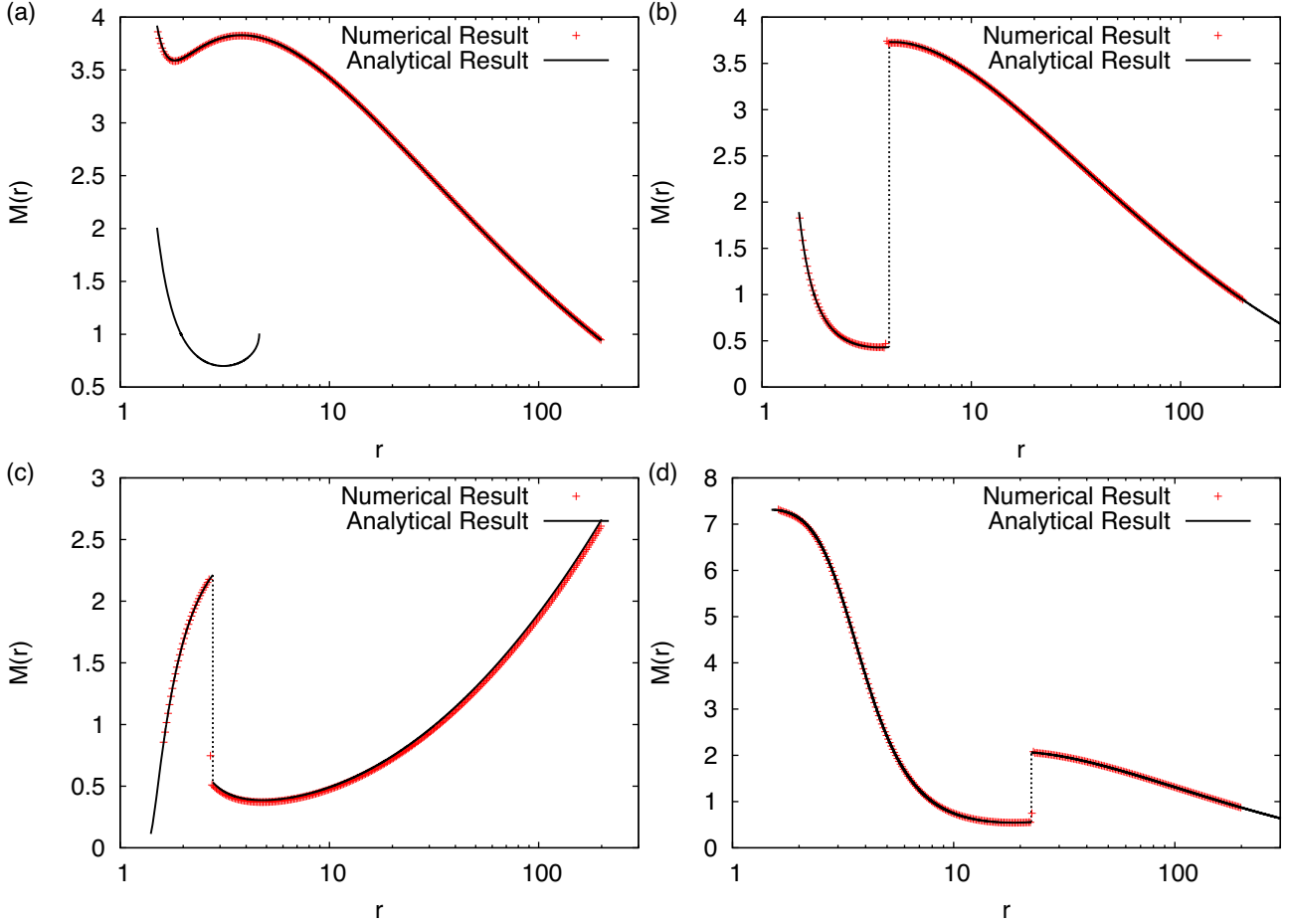


Figure 1. Comparison of radial Mach number (V/a_s) variation for one-dimensional axisymmetric accretion and wind solutions around a rotating black hole. The black solid lines are obtained using analytical method, whereas red points are the simulation results. In (a), we present an accretion solution without a shock. $\varepsilon = 1.004$ and $l = 2.2$ are chosen for this solution (NSA region). (b) An example of an accretion solution where a shock is formed. $\varepsilon = 1.004$ and $l = 2.25$ are chosen for this solution (SA region). According to analytical calculation, shock location is found to be at $r = 4.05$. (c) An example of the wind solution where a shock is formed at $r = 2.77$. The parameters for this solution are $\varepsilon = 1.02$ and $l = 2.3$ (SW region of parameter). The spin parameter $a = 0.95$ for all three cases. (d) An example of an accretion solution where a shock is formed for a retrograde flow. $\varepsilon = 1.004$, $l = 4.0$, and spin parameter $a = -0.95$ are used for this case. Analytically, the shock location is found to be at $r = 22.45$. Numerical simulations clearly captured the shocks exactly where theoretical shock location was predicted.

geometry, Molteni, Lanzafame & Chakrabarti (1994) first carried out this simulation using Smoothed Particle Hydrodynamics (SPH) code and found that a standing shock is formed with an outflow along the polar direction. However, in the context of a complete Kerr geometry the code has never been tested, which formed non-linear shocks right outside a black hole horizon. We take $a = 0.95$ black hole which means the horizon is located at $r = 1.31$. We inject matter at the outer edge at $r = 200$ and the inner absorbing boundary is chosen at $r_{\text{in}} = 1.5$. We choose 300 logarithmically spaced radial grid and 90 equispaced polar grids as before. In Table 1, we present the parameters for all the two-dimensional runs presented here. For run R1, we inject the flow with specific energy and angular momentum $\varepsilon = 1.001$ and $l = 2.25$, respectively. This pair of parameters produces a standing shock when vertical equilibrium model is used (Chakrabarti 1996a). At the outer radius, the injection velocity and sound speed are $V = 0.0634$ and $a_s = 0.0362$ in this case. We run for a time of 2.6×10^4 , which is about 10 times of the in-fall time.

We now show the results, including the initial transient phase when the matter rushed towards the black hole. In Fig. 3(a), we show the inner region of the computational grid to show details of

what happened after quasi-steady state is achieved. We plot density contours superposed with velocity vectors. The length of the arrow is proportional to the logarithm of the velocity magnitude. For a thin flow in a vertical equilibrium, a shock would be expected at $r = 7.5$. However, we are using a geometrically thick flow which after passing through the oblique shock off the equatorial plane, converges towards the black hole and hits the centrifugal barrier and bounce back which then interacts with matter in-flowing on the equatorial plane. This turbulent pressure along with the excess heat generated due to the fall of matter from off the equatorial plane pushes the shock outwards to a distance ~ 22 . Fig. 3 (b) shows the variation of the shock location on the equatorial plane. There is a small amplitude oscillation mostly driven by the inequality between the sum of the pressures in the pre- and post-shock regions. Note the formation of a strong outflow from the surface of the in-flowing post-shock region. Due to dominance of the centrifugal force, this region is also called the CENtrifugal pressure Supported BOundary Layer, or CENBOL, which truly acts like a boundary layer of stars from which winds originate and which up-scatters seed photons to higher energy (Chakrabarti & Titarchuk 1995).

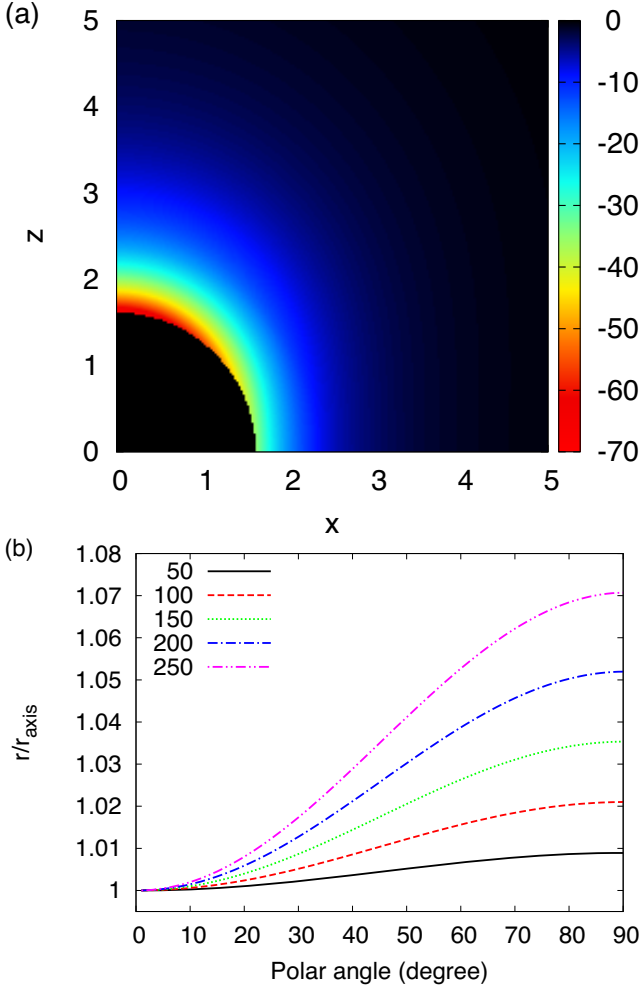


Figure 2. Breaking of symmetry of the flow due to dragging of inertial frame is demonstrated here. (a) Distribution of difference in flow density with identical initial condition at the outer grid at $r = 200$ between a Kerr ($a = 0.95$) black hole and a Schwarzschild ($a = 0$) black hole even if matter is accreted spherically symmetrically far from the central object. We note that while near the equatorial plane the difference is very little, highest difference occurs on the pole. In (b) we plot the contours of constant density in the simulation result as a function of the polar angle and the ratio of the distance (of a given density) divided by the distance (of the same density) along the pole. We see that the same high density 250 occurs on the pole at about 7 per cent distance less than the distance on the equatorial plane. The contours are, from bottom to top, 50, 100, 150, 200, and 250, respectively.

Table 1. Parameters used for the two-dimensional simulations.

Case	ε, l	a	V	a_s
R1	1.001, 2.25	0.95	0.0634	0.0362
R2	1.001, 4.0	-0.95	0.0609	0.0363
R3	1.001, 2.21	0.95	0.0634	0.0362
R4	1.001, 2.63	0.95	0.06299	0.0362

For this case, we can estimate the velocity of the outflowing matter at r_{out} and compare it with the escape velocity of at that radius. The escape velocity at the outer computational domain is

$$v_{\text{esc}} = \sqrt{\frac{2}{r}}. \quad (20)$$

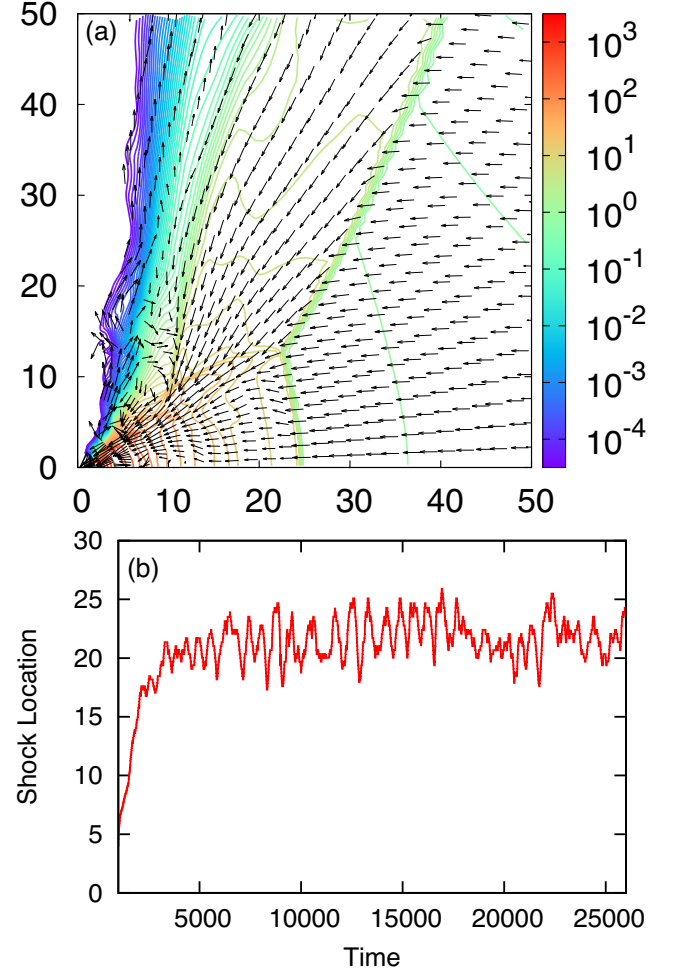


Figure 3. (a) Zoomed snapshot of density contours overplotted with velocity vectors for two-dimensional flow around a Kerr ($a = 0.95$) black hole. The parameters corresponding to run R1 are used. The length of the arrow is proportional to the logarithm of the velocity magnitude. (b) Time variation of shock location on the equatorial plane. A small amplitude oscillation is seen around a mean location ~ 22 . See text for details.

Accordingly, the escape velocity at the computational boundary ($r_{\text{out}} = 200$) is $v_{\text{esc}} = 0.1$. The fluid velocity is given by,

$$v = \sqrt{\gamma_{ij} v^i v^j}. \quad (21)$$

Fig. 4 shows the fluid velocity at the outer boundary as a function of the polar angle for the case R1. The horizontal line shows the escape velocity for the comparison. The numbers show that the fluid velocity is higher than the escape velocity at some locations close to the pole. Near the pole, the fluid actually escapes from the vicinity of the black hole by forming a jet whereas the fluid at all other parts may fall back and become part of the accreting matter. In our case, the outflow is launched from the post-shock region by the combined effects of thermal pressure and centrifugal pressure. As the flow passes through the shock, the matter becomes hotter and entropy rises. This hotter, rotating flow is further squeezed into a small volume due to compression as it further moves towards the black hole. High entropy forces the flow to have the inner sonic point very close to the black hole, where it becomes supersonic. It subsequently expands and expelled in the vertical direction as a strong outflow.

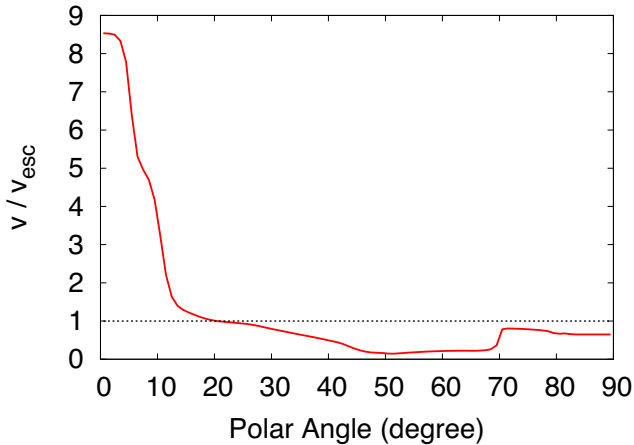


Figure 4. Fluid velocity as a function of polar angle at the computational outer boundary ($r_{\text{out}} = 200$). The dotted horizontal line represents the escape velocity at $r_{\text{out}} = 200$.

In Figs 5(a)–(b) we show analogous results to Fig. 3 when the black hole is spinning in the opposite direction as that of the accretion (run R2). We choose $a = -0.95$ in this case. We choose, $\varepsilon = 1.001$ and $l = 4.0$ which gives $V = 0.0609$ and $a_s = 0.0363$ at $r_{\text{out}} = 200$ for a model flow in vertical equilibrium. We use this velocity to inject matter at the outer boundary. Theoretical location of the shock for these input parameters is 25.8. However, presence of turbulence pushes the shock to about 58. There is also a small amplitude oscillation. Because of the effects of dragging of the inertial frame close to the black hole, forcing the matter to co-rotate with it, there is a large turbulent cell in the CENBOL region. Also note that the oblique and triple shock being weaker in this case, the flow tends to be deflected to form a stronger wind. It is thus possible that the contra-rotating black holes would produce more profuse winds and this phenomenon certainly deserves attention.

Two-dimensional simulations reveal many new aspects of the physics of accretion flows. For instance, the presence of turbulence may change the topology of the solutions altogether. We show example of one such case (run R3) in the next simulation, where we inject a flow which is not supposed to have any standing shock in the vertical equilibrium model (i.e., from the region ‘NSA’ of Chakrabarti 1996a). Here we choose $a = 0.95$ and inject with flow parameters of $\varepsilon = 1.001$ and $l = 2.21$ which gives $V = 0.0634$ and $a_s = 0.0362$ at $r_{\text{out}} = 200$. The flow is injected with this velocity as before. We observe that a shock forms nevertheless, but it does not remain steady. Rather, it exhibits a large amplitude oscillations.

In Figs 6(a)–(b), we plot the density contours superposed with velocity vectors. In Fig. 6(a), the shock is located at ~ 15 while in Fig. 6(b), the shock is located at ~ 20 . In Fig. 6(c), instantaneous shock locations are plotted. This oscillation of shock is very important from the observational point of view, since these are believed to be responsible for QPO of X-rays amplitudes from black hole accretion discs.

In Figs 7(a)–(b) we show results of another case (run R4), where the flow parameter is from ‘O*’ region (Chakrabarti 1996a). The flow parameters are chosen as $\varepsilon = 1.001$ and $l = 2.63$ which yields $V = 0.06299$ and $a_s = 0.0362$ at $r_{\text{out}} = 200$ from the transonic solution. In this case, since the specific angular momentum is larger than the marginally bound value, the steady flow in vertical equilib-

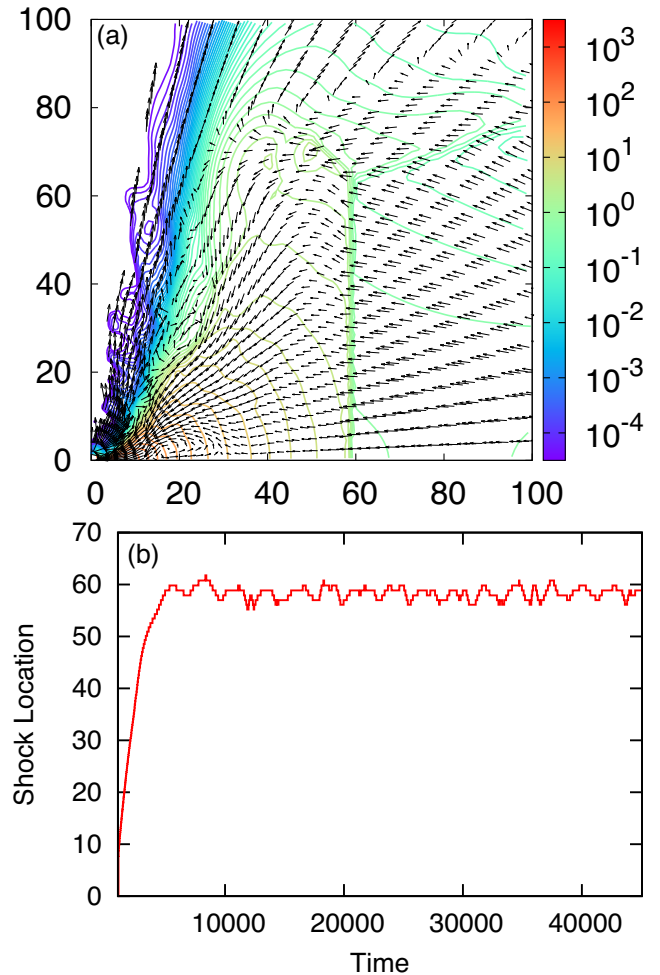


Figure 5. Analogous figure to Fig. 3 for the retrograde case ($a = -0.95$). We choose parameters corresponding to run R2 for this case. Analytically, for these parameters, a steady shock is found to be formed at 25.8. However, in numerical simulation, a shock is found to be formed at ~ 58 .

rium model does not even extend till the horizon and thus a steady flow is impossible. When a time dependent simulation is run we see a very interesting behaviour. The flow is found to be full of turbulence in large and smaller scales, as the branch to enter the black hole is practically blocked due to high centrifugal barrier. Indeed without accretion, and mostly rotating, the isodensity contours assume the shape of thick accretion discs (Paczynski & Wiita 1980; Chakrabarti 1985). The flow tries to enter into the black hole but is unable to do so resulting in accretion of a very little matter. From the simulation, we compute the mass absorption rate, \dot{M}_{abs} , at which the matter is absorbed by black hole through the inner boundary of the computational domain and the mass outflow rate, \dot{M}_{out} , at which the matter leaves the computational domain through the outer boundary as outflow or jet. \dot{M}_{in} measures the mass inflow rate of the incoming matter through the in-flowing boundary.

In Fig. 7(a), we show the contours of constant density superposed with velocity vectors. In Fig. 7(b), the blue curve shows the ratio of the mass absorption rate to the mass inflow rate ($R_{\text{abs}} = \dot{M}_{\text{abs}}/\dot{M}_{\text{in}}$). The red curve shows the ratio of the mass outflow rate to the mass inflow rate ($R_{\text{out}} = \dot{M}_{\text{out}}/\dot{M}_{\text{in}}$). As we can see, nearly no matter is absorbed by the black hole for this case. Instead, almost all the matter is leaving through the outer boundary of the computational

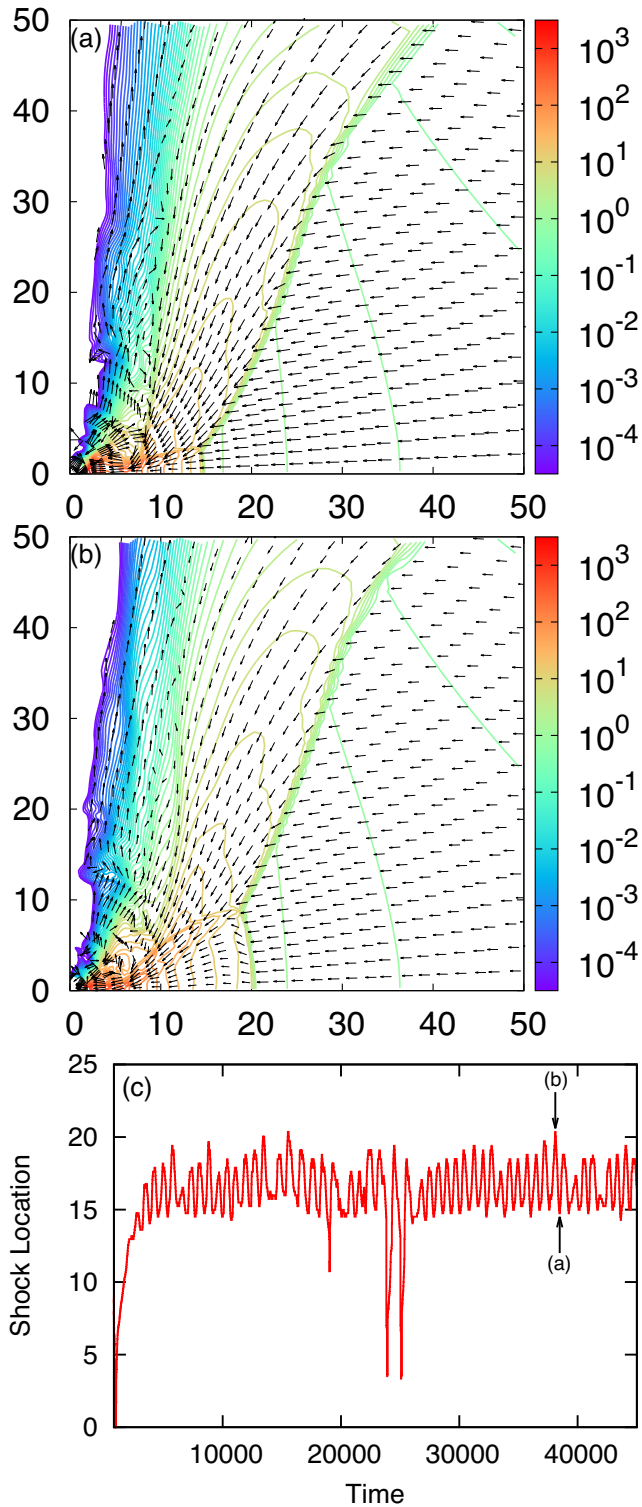


Figure 6. Results of our simulation when the parameters ε and l are not supposed to have shocks in a flow in vertical equilibrium (run R3). (a)–(b): Snapshots of density contours overlplotted with velocity vectors at two different times 38500 and 38100, respectively. The time variation of shock location on the equatorial plane is shown in (c) which show very large amplitude shock oscillations. (a) and (b) are drawn at the times marked by the arrows on (c).

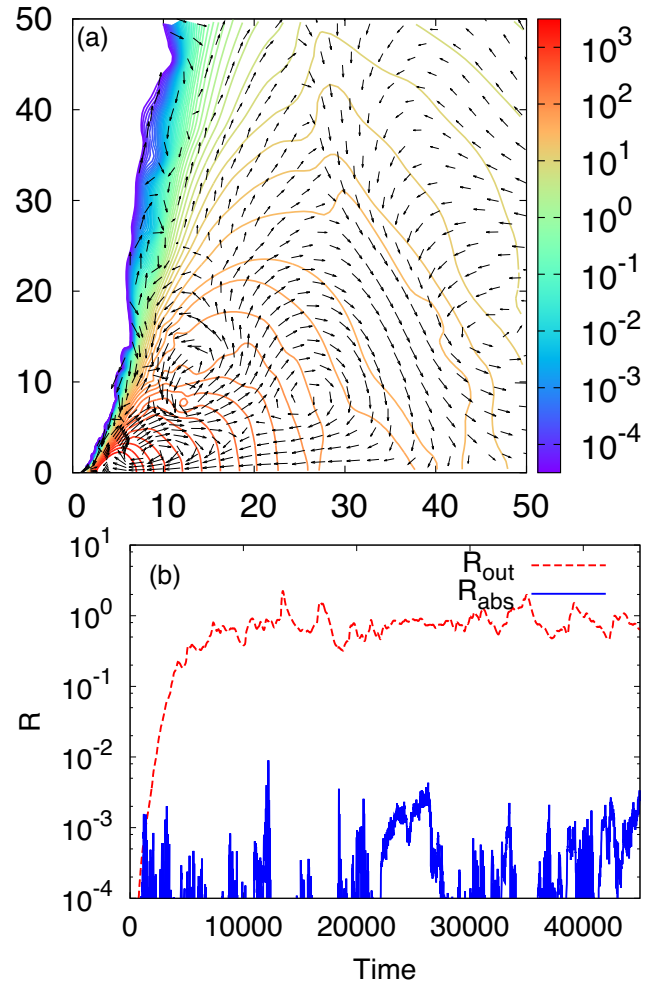


Figure 7. Results of a case with the parameters chosen from O* region (run R4). (a) Density contours overlplotted with velocity vectors showing a thick accretion disc pattern in the absence of accretion. (b) Ratio of the mass absorption rate to the mass inflow rate ($R_{abs} = \dot{M}_{abs}/\dot{M}_{in}$) is shown in blue and Ratio of the mass outflow rate to the mass inflow rate ($R_{out} = \dot{M}_{out}/\dot{M}_{in}$) is shown in red. Nearly no matter is absorbed by the black hole and almost all the matter is leaving through the outer boundary of the computational domain. Occasional $R_{out} > 1$ indicates that the disc is evacuated at that time.

domain (the ratio is around unity for red line). Sometimes, this ratio is more than one showing that the accumulates disc matter may also be evacuated in this case. Fig. 6(b) is drawn in logarithmic scale in order to show small and sudden inflows into the black hole, possibly because of transport of angular momentum of some matter to those leaving the system. Such transports are common in turbulent discs through turbulent viscosity.

For all the cases presented in Table 1, we can estimate Compton y -parameter (Rybicki & Lightman 1979) in the pre- and post-shock regions. Assuming a mass accretion rate ~ 0.1 Eddington rate around a $10 M_{\odot}$ black hole, the values of the Compton y -parameter are found to be $y_{pre-shock} \sim 0.0016$ and $y_{post-shock} \sim 10$. Precisely, such consideration is used to study spectral properties by the TCAF solution (Chakrabarti & Titarchuk 1995).

In our two-dimensional simulations, we also notice the formation of the outflow from the surface of the CENBOL. In order to understand what fraction of injected matter can be swallowed by black hole and what fraction can leave as outflow, we plotted the radial

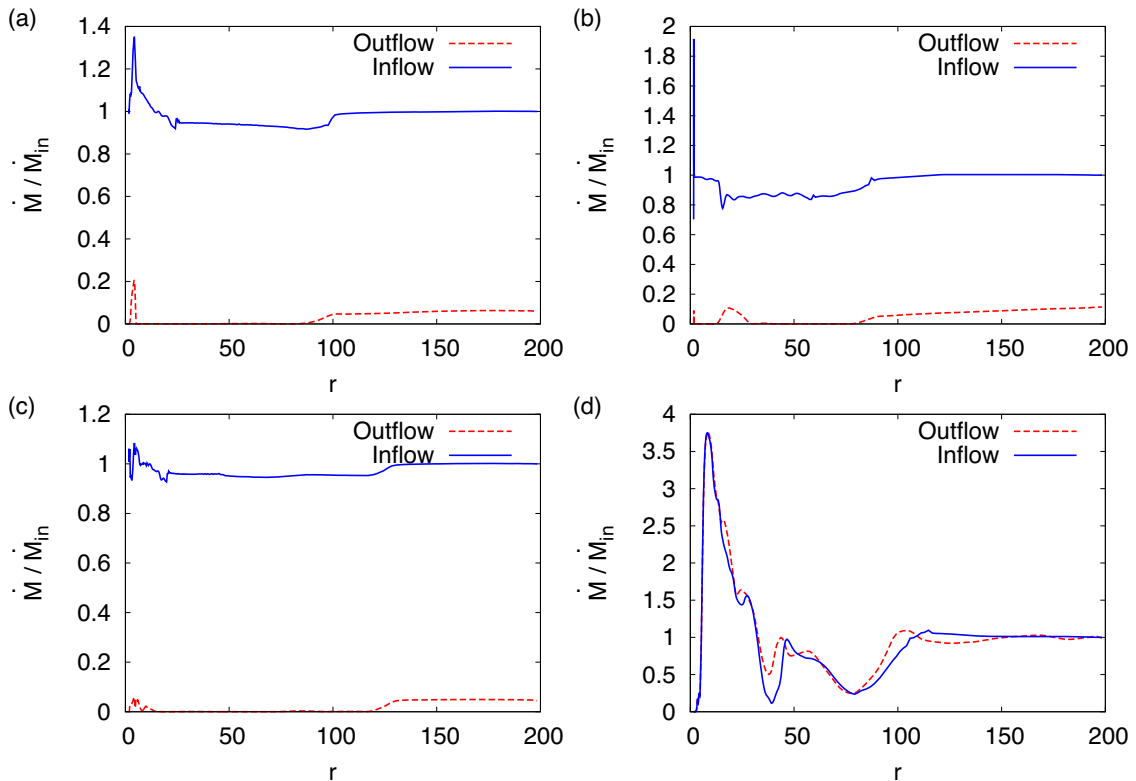


Figure 8. Inflow–Outflow rates, normalized by the mass accretion rate \dot{M}_{in} at r_{out} , as a function of radius for all the cases presented in Table 1. The blue, solid curve shows the inflow rate and red, dashed curve shows the outflow rate. (a), (b), (c), and (d) correspond to cases R1, R2, R3, and R4, respectively.

variation of the corresponding rates for all the four runs presented in Table 1. Fig. 8 shows the results in the steady state for all the cases. In order to find the total inflow rate at a particular radial point, we integrated the inward pointing mass flux in the angular direction at that radius. Similarly, to find the total outflow rate at a particular radial point, we integrated the outward pointing mass flux in the angular direction at that radius. From Figs 8(a), (b), and (c), we find that the flow is mostly accreting at all radii and a small fraction (~ 5 per cent) of injected matter points away from the black hole. Fig. 8(d), on the other hand, shows that at all radii, the inward and the outward mass rate are roughly equal.

Please note that in this paper, our primary goal is to verify whether the numerical solutions are consistent with the theoretical solutions provided in Chakrabarti (1996a,c). During the process, we also find from our simulations that outflow can originate from the post-shock region. Although, our current simulations show that the outflow rate is not significant for the parameters that we use, the rate can be enhanced for accreting flow with higher l (see e.g., Molteni et al. 1994).

5 CONCLUSIONS

Accretion processes on a black hole continues to remain a fascinating subject and with the advent of better observational tools it has become possible to prove models of accretion flows. It is widely understood that an astrophysical black hole may not have any significant Keplerian disc in most of the time and the accretion may be wind driven, i.e., have low-angular momentum. This is especially true for high mass X-ray binaries and active galactic nuclei. It is also found that most of the black holes have spins (see review by

McClintock, Narayan & Steiner 2014). So it is essential to carry out the studies in full Kerr geometry. In the literature, systematic studies have been presented (Chakrabarti 1996a,c) when the low-angular momentum flow is steady and geometrically thin modelled as a conical wedge flow or a flow in vertical equilibrium. However, no theoretical study is either present or possible in Kerr geometry for a geometrically unrestricted flow.

In this paper, for the first time, we present results of a fully general relativistic flow. We first tested the code in one dimension (i.e. on the equatorial plane) and showed that the code exactly reproduced the corresponding flow solutions with and without a shock transition, in both accretion and winds. We then applied the code for a two-dimensional Bondi flow and found that due to dragging of the inertial frame, even a spherically symmetrically injected flow at the outer grid boundary takes an oblate shape and the isodensity contours show this deformity. Finally, we ran several cases of two-dimensional flows with finite specific angular momentum. We chose input parameters and compared the results with steady solutions from vertical equilibrium model. We discover that turbulent pressure is much stronger for a rapidly spinning black hole and pushes the shock by a large amount. This effect was much weaker in Schwarzschild black hole modelled with pseudo-Newtonian potential (Molteni et al. 1994). We also carried out simulations with contra-rotating black holes and show that the flow is very turbulent close to the horizon, especially because of the dragging of matter in the opposite direction by the black hole. We also showed that because of this turbulence, the shock is located much further out. Finally, we considered a case which is not supposed to be accreting according to vertical equilibrium model. Indeed, we find that the accretion is very low and almost all the matter is ejected as winds, often partially evacuating the disc itself when the outflow rate is

higher than the inflow rate. In a realistic and generalized accretion process scenario on a black hole, one often finds signatures of two components where the viscous accretion discs are surrounded by low-angular momentum flows such as those we used in this paper (Chakrabarti 1996b; Giri & Chakrabarti 2013; Chakrabarti et al. 2015; Giri, Garain & Chakrabarti 2015). In future, our goal would be to introduce viscosity and radiative processes to produce self-consistent spectrum out of discs around a rotating black hole. In that case the spin parameter may also be determined from the value of frequency at which the shocks oscillate. These would be carried out in future.

ACKNOWLEDGEMENTS

DSB acknowledges support via National Science Foundation grants NSF-ACI-1533850, NSF-DMS-1622457, and NSF-ACI-1713765. Several simulations were performed on a cluster at University of Notre Dame that is run by the Center for Research Computing. Computer support on NSF's XSEDE and Blue Waters computing resources is also acknowledged. JK also acknowledges support by the National Research Foundation of Korea grant NRF-2018R1D1A1B07042949.

REFERENCES

- Arnowitt R., Deser S., Misner C. W., 2008, *Gen. Relativ. Gravit.*, 40, 1997
- Banyuls F., Font J. A., Ibáñez J. M., Martí J. M., Miralles J. A., 1997, *ApJ*, 476, 221
- Bhattacharjee A., Banerjee I., Banerjee A., Debnath D., Chakrabarti S. K., 2017, *MNRAS*, 466, 1372
- Boyer R. H., Lindquist R. W., 1967, *J. Math. Phys.*, 8, 265
- Chakrabarti S., Titarchuk L. G., 1995, *ApJ*, 455, 623
- Chakrabarti S. K., 1985, *ApJ*, 288, 1
- Chakrabarti S. K., 1989, *ApJ*, 347, 365
- Chakrabarti S. K., 1996a, *MNRAS*, 283, 325
- Chakrabarti S. K., 1996b, *ApJ*, 464, 664
- Chakrabarti S. K., 1996c, *ApJ*, 471, 237
- Chakrabarti S. K., Acharyya K., Molteni D., 2004, *A&A*, 421, 1
- Chakrabarti S. K., Mondal S., Debnath D., 2015, *MNRAS*, 452, 3451
- Chatterjee D., Debnath D., Chakrabarti S. K., Mondal S., Jana A., 2016, *ApJ*, 827, 88
- Debnath D., Chakrabarti S. K., Mondal S., 2014, *MNRAS*, 440, L121
- Debnath D., Jana A., Chakrabarti S. K., Chatterjee D., Mondal S., 2017, *ApJ*, 850, 92
- Garain S. K., Ghosh H., Chakrabarti S. K., 2014, *MNRAS*, 437, 1329
- Giri K., Chakrabarti S. K., 2013, *MNRAS*, 430, 2836
- Giri K., Garain S. K., Chakrabarti S. K., 2015, *MNRAS*, 448, 3221
- Harten A., Lax P. D., van Leer B., 1983, *SIAM Rev.*, 25, 35
- Kim J., Kim H. I., Choptuik M. W., Lee H. M., 2012, *MNRAS*, 424, 830
- Kim J., Garain S. K., Balsara D. S., Chakrabarti S. K., 2017, *MNRAS*, 472, 542
- McClintock J. E., Narayan R., Steiner J. F., 2014, *Space Sci. Rev.*, 183, 295
- Michel F. C., 1972, *Ap&SS*, 15, 153
- Molteni D., Lanzafame G., Chakrabarti S. K., 1994, *ApJ*, 425, 161
- Molteni D., Sponholz H., Chakrabarti S. K., 1996, *ApJ*, 457, 805
- Novikov I. D., Thorne K. S., 1973, in Dewitt C., Dewitt B., eds, *Black Holes (Les Astres Occlus)*, Gordon and Breach, New York, p. 343
- Paczynski B., Wiita P. J., 1980, *A&A*, 88, 23
- Rybicki G. B., Lightman A. P., 1979, *Radiative processes in astrophysics*, Wiley, New York
- Shibata M., 2003, *Phys. Rev.*, 67, 024033
- Shu C.-W., Osher S., 1988, *J. Comput. Phys.*, 77, 439

This paper has been typeset from a $\text{\TeX}/\text{\LaTeX}$ file prepared by the author.